

1  
2  
3  
4  
5  
6  
7  
8  
9  
10  
11  
12  
13  
14  
15  
16  
17  
18  
19  
20  
21  
22  
23  
24  
25  
26  
27  
28  
29  
30  
31  
32  
33  
34

# Experimental study of detonation limits in methane-oxygen mixtures: Determining tube scale and initial pressure effects

Bo Zhang<sup>1\*</sup>, Hong Liu<sup>1†</sup>, Bingjian Yan<sup>2</sup>, Hoi Dick Ng<sup>3</sup>

<sup>1</sup>Shanghai Jiao Tong University  
School of Aeronautics and Astronautics, Shanghai, 200240, China

<sup>2</sup> East China University of Science and Technology  
School of Resources and Environmental Engineering, Shanghai, 200237, China

<sup>3</sup> Concordia University  
Department of **Mechanical, Industrial and Aerospace Engineering**  
Montréal, **QC**, H3G 1M8, Canada

## Corresponding Authors

E-mail:

\*bozhang@sjtu.edu.cn; zhangb@live.cn (B. Zhang)

†hongliu@sjtu.edu.cn (H. Liu)

## Abstract

35  
36  
37  
38  
39  
40  
41  
42  
43  
44  
45  
46  
47  
48  
49  
50  
51  
52  
53  
54  
55  
56  
57  
58  
59  
60  
61

In this paper, **detonation limits in stoichiometric methane-oxygen mixtures** with varying tube inner diameter and **initial mixture pressure** were investigated. Detonations in tubes with different inner diameter ( $D = 36$  mm, 25 mm, 20 mm and 13 mm) and low initial pressure from 3.5 ~ 18 kPa were studied. Smoked foils were applied to observe the evolution of the detonation cellular structure for various initial conditions. An alternate length scale **at the limits** is examined,  $L_{\text{dcs}}$ , which is the maximum length from the beginning of the test section after which cellular patterns can no longer be observed. Simultaneous local velocity measurements were obtained by photodiodes to complement the  $L_{\text{dcs}}$  results. The study **also** aims to reveal relation between the near-limit detonation dynamics, the tube geometry, and the thermodynamic properties of the mixture. **Past the failure** limit,  $L_{\text{dcs}}$  decreases with decreasing **initial mixture pressure** for a given tube diameter, and  $L_{\text{dcs}}$  decreases faster in a smaller diameter tube. In the  $D = 13$  mm tube, galloping detonation mode is observed, and the length of the galloping cycle is reduced with an increase in initial pressure. To further **characterize the onset of detonation limits**, a scaling analysis of  $L_{\text{dcs}}$  with tube inner diameter ( $D$ ) and detonation cell size ( $\lambda$ ) was performed. The experimental results show that the decrease of  $L_{\text{dcs}}/D$  and  $L_{\text{dcs}}/\lambda$  are more abrupt in smaller diameter tubes with decreasing initial pressure. At low initial pressure, the boundary layer displacement thickness growth is significant in the flow structure. Since the distribution of global curvature over the whole detonation front is faster in smaller tube, it thus leads to a more abrupt decrease sensitive to initial pressure. For increasing pressure closer to the critical failure limit, the boundary layer displacement thickness is becoming less comparable to the tube diameter. The failure mechanism appears to be more dominant by the rate of transverse waves attenuation or cell disappearance. Lastly, by comparing the detonation cell size and the tube scale at the critical limits condition in different tubes,  $\lambda = \pi \cdot D$  is shown to be an appropriate limit criterion of detonation propagation in agreement previous studies.

**Keywords:** Detonation limits; Tube inner diameter; Initial pressure; Detonation cellular structure

## 62 1. Introduction

63 An explosion is the result of a rapid expansion of product gases, for example, from a  
64 combustion process. Explosion is a high energy release process and it creates a blast wave,  
65 whether this wave decays to sub- or supersonic depends on the amount of energy released. In  
66 the subsonic case, explosions are created by the ignition and subsequent slow burning of  
67 combustibles known as deflagration. In the supersonic case, explosions result when the  
68 combustion occurs in the detonation regime. A detonation is a supersonic, combustion-driven,  
69 compression wave. Ideally, the detonation structure is described by a lead shock followed by a  
70 reaction zone consisted of an induction followed by the exothermic energy release. It is a  
71 supersonic combustion with an overpressure of about 20~30 times the initial pressure and a  
72 propagation velocity of about 2~3 km/s. Real detonations have a three dimensional cellular  
73 structure, this complicated structure comprises of transverse waves, triple-points, and turbulent  
74 shear layers [1-3].

75 For the past century, investigations on detonation dynamics have attracted numerous  
76 researchers mainly due to two aspects. First is to prevent and mitigate the formation of  
77 detonations in industrial processes. From a safety point-of-view, only by knowing the critical  
78 conditions that the detonation initiation or failure then can the corresponding safety precautions  
79 be effectively formulated [4]. The second aspect is to develop potential detonation-based  
80 propulsion systems and harnesses their high propulsive efficiency. Examples include pulse  
81 detonation engines [5-8], rotating detonation engines [9-11] and oblique detonation wave  
82 engines [12-19].

83 Soon after the discovery of the detonation phenomenon, Chapman and Jouguet proposed a  
84 theory that quantitatively calculated the detonation velocity of a combustible mixture, known as

85 Chapman–Jouguet (CJ) theory. However, the CJ theory suggests that the detonation velocity  
86 depends only on the thermodynamic properties of the mixture, but independent of detonation  
87 wave structure and boundary conditions. Therefore, for a detonation propagating in a given  
88 mixture and confining environment, the self-sustained propagation state can always be  
89 maintained regardless of the tube geometry and other boundary conditions. In reality, however,  
90 the propagation of detonations is strongly affected by the boundary conditions; this is owing to  
91 the detonation vulnerable to boundary effects because of its finite thickness of the reaction zone  
92 [20]. In general, the boundary effects result in a velocity deficit and further render the  
93 detonation to decay, and finally approach the detonation limits leading to failure.

94  
95 Table. 1 Previous literature of detonation propagation limits

No.	Authors	Year	Tube length/m	$D$ or $H$ /mm	$(L/D, L/H)_{\max}$
1.	Ishii & Grönig [21]	1998	14	45	311.1
2.	Haloua et al. [22]	2000	24.5	38	644.7
3.	Ishii et al. [23]	2002	5.05	50.5	100
4.	Chao et al. [24]	2009	3	CT:65, AC:2.2/6.9	1363.6
5.	Kitano et al. [25]	2009	3	3/6/10	1000
6.	Camargo et al. [26]	2010	3	1.8/ 6.3/ 9.5	1666.7
7.	Ishii & Monwar [27]	2011	5.05	50.5	100
8.	Sadahira et al. [28]	2013	5	3.1/ 6.0/ 8.8	1612.9
9.	Lee et al. [29]	2013	4.16	CT:13/44/65, AC:3.175/6.35/9.525	1310.2
10.	Gao et al. [30-34]	2014-2016	2.438/4.118	1.5/3.2/12.7/31.7/ 50.8	2745.3
11.	Wu & Lee [35]	2015	3	50.8	59.1
12.	Yoshida et al. [36]	2016	6	5.8/8/10	1034.5
13.	Jackson et al. [37]	2016	30	4.1	7317.1
14.	Wang et al. [38]	2017	2.5	32	78.1
15.	Zhang et al. [34, 39-50]	2015-2019	2.5	CT:4/14/36, AC:2/4.5/7	1250

96

97 Detonation limits is a fundamental dynamic parameter of detonations [39, 40, 43, 48, 51].

98 As the detonation limit is reached, a variety of unstable propagation phenomena occur, e.g.,

99 galloping detonations, spinning detonations, and stuttering detonations. Detonation limit  
100 conditions are reached through reducing the initial pressure of the combustible mixture,  
101 changing the confinement geometry and/or scale, increasing the amount of an inert diluent,  
102 changing the roughness of the confinement boundary, etc. For reference, a number of  
103 investigations regarding detonation limits in recent years are tabulated in Table.1.

104 Although similar detonation tubes with circular or annular geometries have been normally  
105 used, the tube configuration (e.g., tube length, or the ratio between the length and inner diameter  
106  $L/D$ ) is quantitatively different (as shown in Table.1). Therefore, the critical condition (e.g.,  $p_c$  -  
107 critical pressure) of detonation propagation limit for each apparatus also varies. For example,  
108 Wu and Lee [35] reported the maximum initial pressure of  $\text{CH}_4 + 2\text{O}_2$  mixture at which spinning  
109 detonations failed was 4.3 kPa, in which they employed a polycarbonate tube of 50.8 mm in  
110 diameter and 3 m long. However, a pressure value of 3 kPa was found by Zhang et al. [46] for  
111 the same mixture, but in a tube of 36 mm in diameter and 2.5 m long. Generally, the detonation  
112 limit is preceded by a detonation velocity deficit. Previous studies [34, 47, 52] have suggested  
113 that the mechanism of the velocity deficit can be attributed to the flow divergence that caused  
114 by the boundary layer effect in small tubes. Besides, the velocity deficit can also be caused by  
115 the effect of momentum and heat losses to the wall [24, 25]. Therefore, it is reasonable to  
116 speculate that the critical pressure for self-sustained detonations in tubes with different  
117 geometries should also be different. To this end, a universal criterion of detonation limits that  
118 considers the tube geometry and initial mixture conditions is desirable.

119 For a given duct, as the initial pressure is well above the detonation limit, the wave can  
120 self-sustainably propagate, and its velocity is usually steady. The detonation limit can be  
121 reached though gradually reducing the initial pressure, whereby the cellular structure vanishes

122 completely after a distance from the beginning of the tube, and the detonation velocity starts to  
123 decay. With decreasing initial pressure, the combustion mode turns into a fast deflagration  
124 regime. On the other hand, for a given mixture and initial pressure, detonations are more  
125 affected by smaller diameter tubes, and the detonation wave fails after a shorter distance if the  
126 tube diameter is reduced. Although the above behaviors can be qualitatively presumed,  
127 nevertheless, the quantitative relationship between the detonation propagation distance with the  
128 independent effects from tube inner diameter and the initial pressure of mixture are interesting  
129 to be investigated. In industry that involves the use of chemical processes, this quantitative  
130 relationship of detonation limit with those factors is important for the designers to take effective  
131 measures to prevent the formation or transmission of a detonation in pipes and ducts. In addition,  
132 this quantitative relationship is also meaningful for the engineers that investigate the  
133 detonation-based propulsion devices, in which the detonation is expected to be maintained and  
134 has to be away from the limit conditions to keep the thrust ability as an engine.

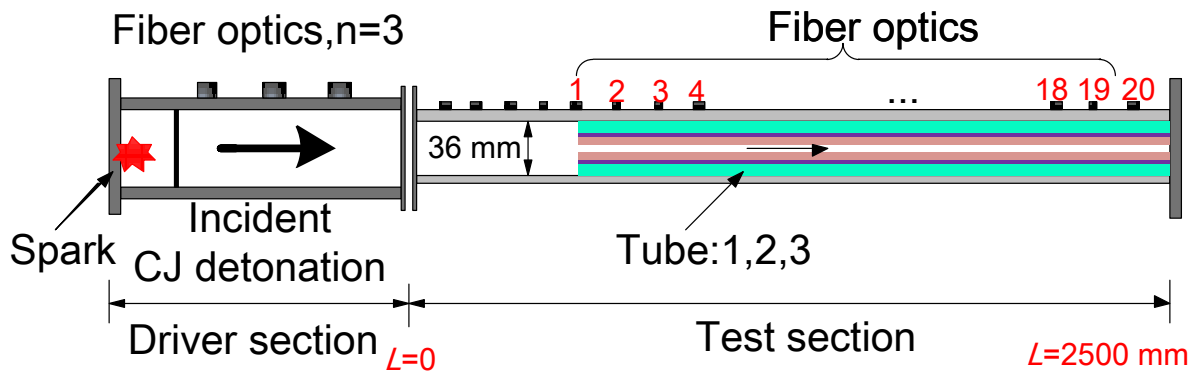
135 In this study, detonation experiments were performed in tubes with four inner diameters  
136 (i.e.,  $D = 36, 25, 20$  and  $13$  mm). The detonation cellular patterns and wave velocities were  
137 simultaneously recorded at varying initial pressures. In order to examine the results, an alternate  
138 length scale is considered. The maximum length of detonation cellular structure ( $L_{dcs}$ ), defined  
139 as the length from the start of the test tube section to the location where no detonation cellular  
140 pattern is observed, was obtained for each condition to explore the quantitative effects of tube  
141 geometry and the thermodynamic properties of the mixture on the detonation limit. It is worth  
142 noting that similar characteristic length was also used in Radulescu and Lee [53] to define the  
143 failure limit in porous walled tubes. They reported a failure length, and this length can be  
144 approximately considered a constant, of the order of 3 to 7  $\lambda$ . The failure is mainly due to the

145 losses and mass divergence into the porous walls and not inherently by the tube scale or  
 146 geometry. The porous walled tubes not only attenuate transverse waves and the global mass  
 147 divergence into the permeable walls introduces curvature slowly disturbed in the leading front.

148

## 149 2. Experimental Details

### 150 2.1 Experimental apparatus



151

152 Fig.1 Schematic diagram of the experimental device

153

154 **Detonation limits experiments** were performed in a detonation tube facility 3700 mm in length.

155 It comprised **both** driver and driven sections, a diaphragm ( $L = 0$ ) was used to separate these two

156 sections. The driver section is 1200 mm in length and 68 mm in inner diameter, the test section is

157 2500 mm in length and 36 mm in inner diameter, as shown schematically in Figure. 1. Equi-molar

158  $C_2H_2 + O_2$  **was** used as driver mixture, it is very sensitive and readily forms a CJ detonation, and the

159 initial pressure was 10 kPa. The test section was filled with the desired test mixture ( $CH_4 + 2O_2$ ).

160 Various transparent acrylic glass tubes with smaller diameter were inserted into the test section,

161 which were used to change the test section's inner diameter. The inner diameters ( $D$ ) of the tubes

162 (No. 1, 2, 3) were 25 mm, 20 mm and 13 mm, respectively. All the glass tubes were 2000 mm in

163 length (i.e., from  $L = 500$  mm to  $L = 2500$  mm). **The initial pressure and tube diameter were two**

164 important parameters that affect the detonation propagation limits. The initial pressure affects the  
165 characteristic scale of the detonation structure, while the tube diameter is related to the physical  
166 length scale of the boundary. The initial pressure is also a controlling variable to approach the  
167 detonation limits. In this study, a certain discrimination of tube inner diameter was required, i.e.,  
168 from large (36 mm) to small (13 mm). The sizes are chosen such that the critical pressure for the  
169 limits will be within the range of safety for the present detonation facility. The selection of initial  
170 pressure was mainly dependent on the width of detonation cellular structure. In some cases, as the  
171  $p_0$  is relatively high, an entire soot foil recorded with cellular structure can be observed, indicating  
172 the condition is well within the detonation limit. Hence, any higher initial pressure is irrelevant for  
173 the present investigation on detonation limits.

174 In this study,  $L_{\text{dcs}}$  refers to the length from the start of the test section to the location where no  
175 detonation cellular pattern is observed. As shown in Fig. 1 the test section comprises two parts, the  
176 first part is a short length section ( $L_1 = 500$  mm) prior the glass tube. The purpose of this section is  
177 ensure a well-established detonation is formed in the test mixture. Without this part, the detonation  
178 in the entrance of small tube could be from the driver mixture. To eliminate this possibility, this  
179 buffer section is necessary. The second part is the small glass tube section ( $L_2 = 2000$  mm). In fact,  
180 it is possible in the definition of  $L_{\text{dcs}}$  to eliminate the constant length  $L_1 = 500$  mm since the  
181 detonation only fails in the small glass tubes for all test conditions. Thus, all the  $L_{\text{dcs}}$  values will be  
182 simply shifted by a constant and such consequence will not affect the conclusion of this work.  
183 However, there are two reasons why  $L_1$  is kept in the  $L_{\text{dcs}}$ . First, both  $L_1$  and  $L_2$  sections were filled  
184 with the same mixture at which a detonation propagates and that the detonation in the small tube is  
185 not directly initiated, but rather it transmits from a bigger inner diameter tube. In other words, the  
186 detonation has already established before the entrance of small tube, hence the detonation



187 propagation distance before it goes into the small tube should be considered. Second, for  
188 completeness, the inclusion of  $L_1$  in the present  $L_{\text{dcs}}$  definition can take into account possible losses  
189 in this first section particularly for cases with very low initial pressure conditions. Nevertheless, the  
190 latter may not be as significant since limits are reached far before in the small glass tubes.

191 It is also worth mentioning that, to minimize any shock wave reflection of the detonation  
192 front from the step change as it enters into a reduced small area, Xiao et al. [54] used a protruded  
193 rounded tip at the entrance. In this study, the area step change is not as severe as in [54]. It is also  
194 challenging to modify smoothly the entrance of the small tubes section. Hence, the transparent  
195 acrylic glass tubes used in this study are with a flat straight cutting edge. Although this  
196 configuration unavoidably results in shock reflection at the entrance of acrylic glass tubes and that  
197 the shock reflection may affect the early initial transient of detonation behavior in the small tubes, it  
198 provides a consistent initial condition for all tests. To significantly avoid any shock reflection  
199 resulted from the step change, a long gradual rounded ramp must be used. However, the latter will  
200 generate even much different initial conditions for each test as it allows the cellular detonation to  
201 adjust to different structure. Any roughness from any imperfect modification will also perturb the  
202 detonation entering the small tubes.

203 In the experiment, cellular detonation pattern was recorded by smoked foil technique. To  
204 obtain records of the cellular pattern in the test section, the foil was placed along the internal face of  
205 tube (typically  $L = 500 \text{ mm} - 2500 \text{ mm}$ ).

206 In addition, the combustion wave velocity was also determined to observe the attenuation of  
207 the detonation propagation. The local wave velocity was obtained by computing the length over two  
208 adjacent arrival time signals; these signals were generated from optical fibers together with  
209 photodiode. In the test section, twenty-four fibers equally distributed, and the distance between each

210 other was 10 cm. Figure 1 shows 20 optical fibers from  $L = 500$  mm to 2500 mm, and 4 more fibers  
211 were placed before  $L = 500$  mm.

212

## 213 2.2 Experimental uncertainty

214 The uncertainties of experimental measurement were from two aspects: a) initial pressure  
215 measurement, and b) the determination of the length ( $L_{dcs}$ ). Methane and oxygen at equivalence  
216 ratio  $\varphi=1$  was used in this work, and  $T_0=300$  K. The mixture was prepared by the partial pressure  
217 method in a 40-L high pressure mixing bottle and allowed to mix by diffusion for at least 24 h to  
218 ensure the homogeneity prior to be used. The bottle was initially evacuated to an absolute pressure  
219 of 0.1 kPa. It was then filled with the fuel (i.e., methane) to the desired pressure. For the  
220 stoichiometric condition, i.e.,  $\varphi = 1$  ( $\text{CH}_4:\text{O}_2 = 1:2$ ), the mixing bottle was filled with the fuel to 60  
221 kPa and afterwards, with oxygen into the bottle up to the 180 kPa desired initial mixture pressure in  
222 the mixing bottle. The gas handling was monitored by the OMEGA PX309 pressure gauge. Before  
223 each experiment, the detonation tube was first evacuated and then filled with the mixture from the  
224 high pressure mixing bottle directly. The initial pressure in the mixing bottle and detonation tube  
225 was measured by OMEGA pressure gauges (shown in Table 2). Table 2 gives the accuracy and  
226 maximum error of each gauge.

227

228 Table.2 The accuracy and maximum error of sensors

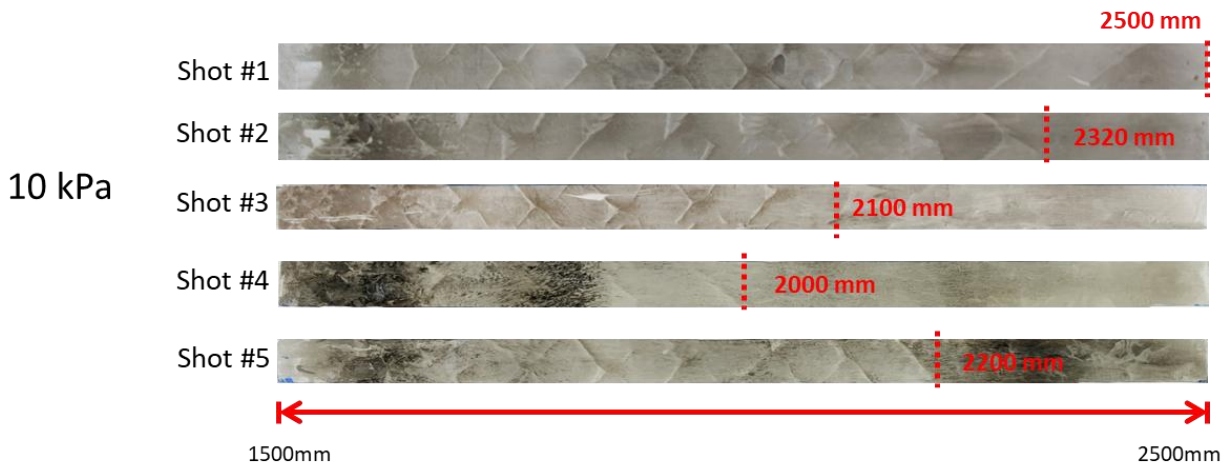
Type	Range/PSI	Accuracy	Maximum Error/ kPa
PX309	0-200	$\pm 0.25\%$	$\pm 3.45$
HHP242	0-30	$\pm 0.10\%$	$\pm 0.20$

229

230 Besides the pressure monitoring, uncertainties in smoked foils measurement also arose due to  
231 the unstable nature of detonation waves. It has been established that detonation waves are

232 essentially unstable and possess a transient 3-D structure, even though the global velocity is still  
 233 close to the one-dimensional steady CJ velocity. Based on the regularity of the detonation cellular  
 234 pattern and the stability parameter  $\chi$ , Radulescu [55] and Ng [56] classified **qualitatively** various  
 235 mixtures into several types, i.e., stable, mildly unstable and highly unstable. Accordingly, CH<sub>4</sub> +  
 236 2O<sub>2</sub> is one of the typical unstable mixtures and has very irregular cellular pattern. Note that  $\chi$  is a  
 237 dimensionless parameter, which is used to characterize the detonation stability. For unstable  
 238 mixtures, their values of  $\chi$  are found to be much larger than stable mixtures (e.g., highly argon  
 239 diluted mixtures). For the latter mixtures, their cellular pattern are regular.

240 The measurements of  $L_{dcs}$  were conducted in different tubes. Five shots were performed at the  
 241 same initial condition for the CH<sub>4</sub> + 2O<sub>2</sub> mixture, i.e.,  $D = 25$  mm,  $p_0 = 10$  kPa. The smoked foils (1  
 242 m in length) with the same thickness (0.1 mm) were inserted from  $L = 1500$  mm to 2500 mm (See  
 243 Fig. 2). From Fig. 2, the longest distance  $L_{dcs}$  was 2500 mm, and the shortest distance was 2000 mm,  
 244 with an average value of 2220 mm, standard error of 86.02 mm ( $\pm 3.87\%$ ). The statistics of  
 245 experimental uncertainty was illustrated in Fig. 3.



246  
 247 Fig. 2 Smoked foils obtained from the repeatability shots at the same condition  
 248 ( $D=25$  mm,  $p_0=10$  kPa)  
 249

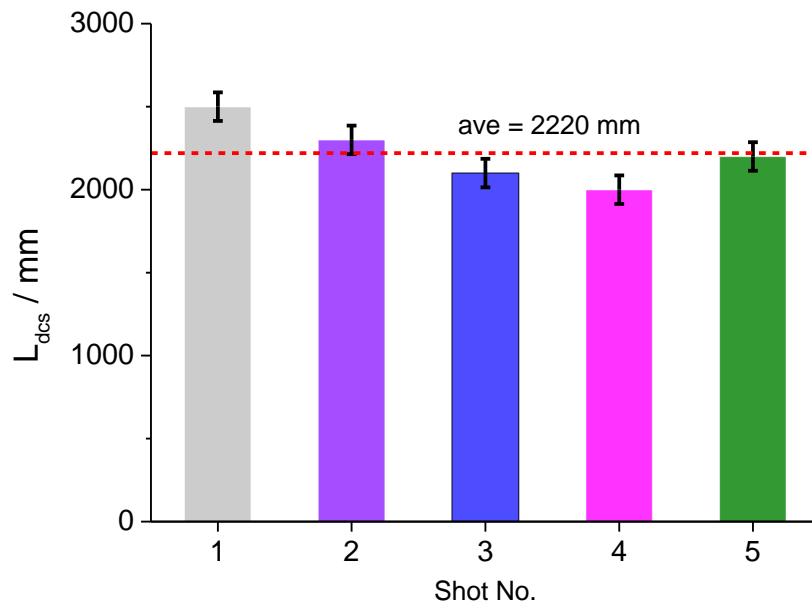


Fig.3 Experimental uncertainty of  $L_{dcs}$

250  
251  
252  
253  
254  
255  
256  
257  
258  
259

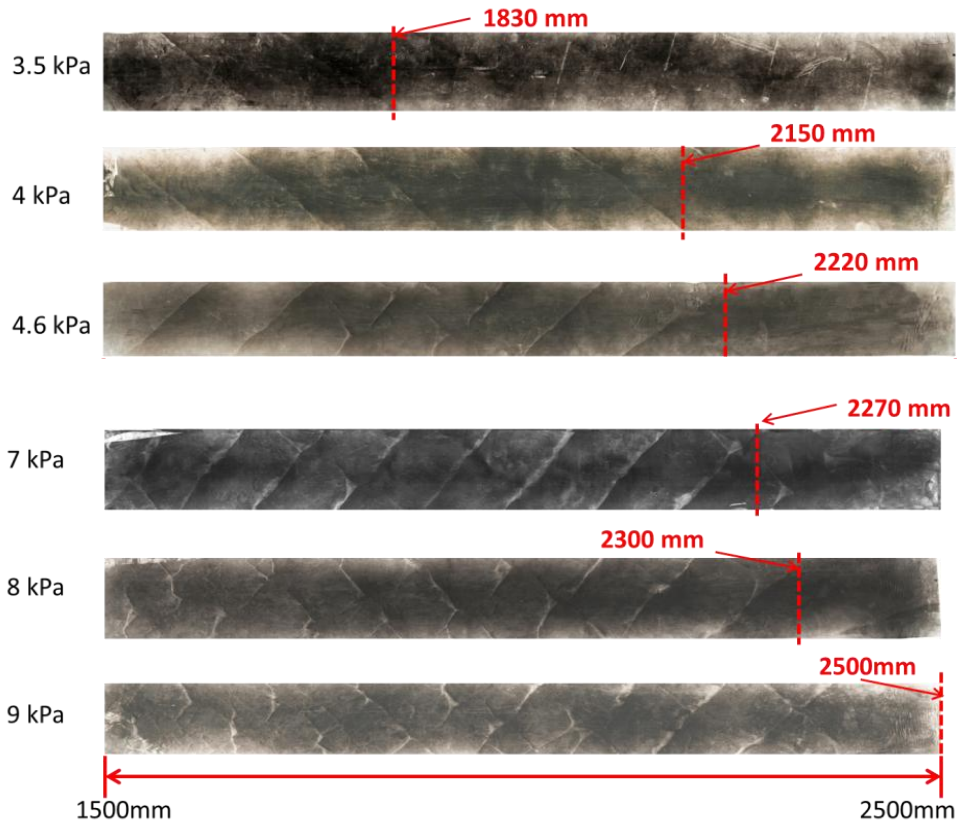
In addition, the uncertainty of the velocity should be considered. The response time (output rise or fall) of the fiber optic detector (IF-95OC) is  $0.1 \mu\text{s}$ . Since the distance between each optical fiber is 10 cm, if it is a CJ detonation (e.g.,  $V_{CJ}=2280 \text{ m/s}$  at  $p_0=8 \text{ kPa}$ ), the interval time between two adjacent fibers is  $43.86 \mu\text{s}$ , if the response time of the optics is considered, the error of the velocity measurement is 0.44%.

260

### 261 3. Results and discussions

#### 262 3.1 Maximum length of detonation cellular structure ( $L_{dcs}$ )

263



264

265

Fig. 4 Detonation cellular pattern in the  $D = 36$  mm tube with the variation of  $p_0$

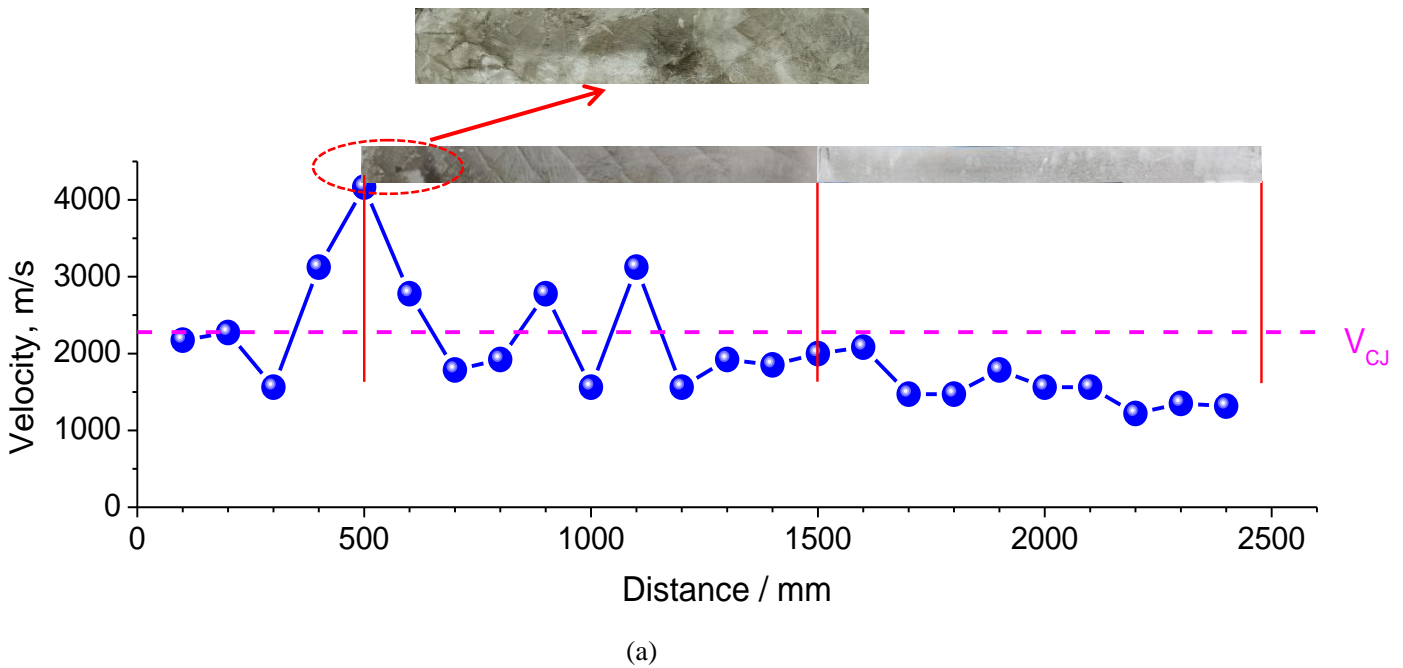
266

267 Figure 4 shows the results of  $L_{dcs}$  for the  $\text{CH}_4 + 2\text{O}_2$  mixture in a  $D = 36$  mm circular tube  
268 under various initial pressures. At  $p_0 = 3.5$  kPa, the detonation structure first appears as a  
269 single-headed spin, which is the typical behavior as the detonation is approaching its limit. For this  
270 case,  $L_{dcs} = 1830$  mm, after which no cellular structure can be found. The latter indicates that the  
271 precursor shock decouples from the following reaction zone and hence, the failure of detonation  
272 occurs. After  $L_{dcs} = 1830$  mm, there are still some weak helical traces that appear seemingly, those  
273 are not representative of detonation structure, but only faint pressure waves pattern that reflected  
274 from the tube wall or soot displaced by the flame.

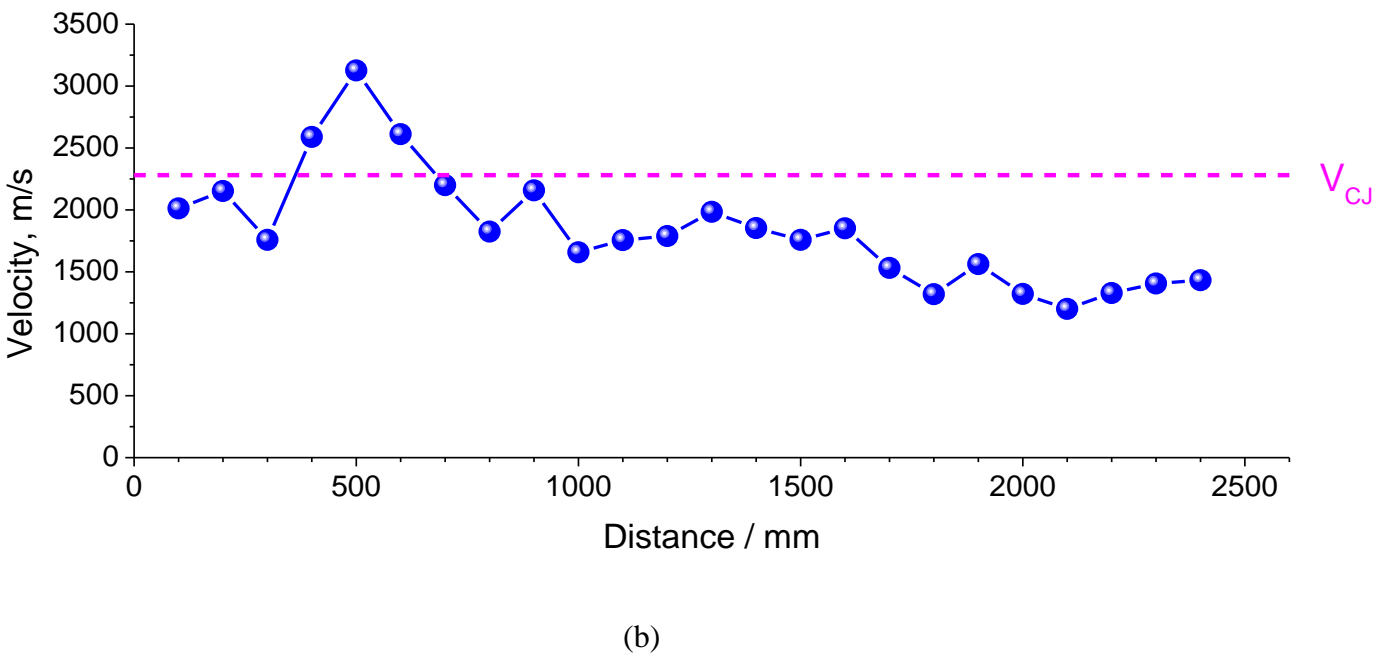
275 For initial pressures below 9 kPa, cellular patterns can be observed only in part of the smoked  
 276 foil, the propagation length of  $L_{dcs}$  is longer at higher initial pressure. At  $p_0 = 9$  kPa, cellular patterns  
 277 are registered on the complete foil and therefore, the critical pressure ( $p_c$ ) for the 36-mm circular  
 278 tube is accordingly 9 kPa. As  $p_0$  increases higher than 9 kPa, it can be speculated that the detonation  
 279 can be self-sustained in the current tube.

280

281  
 282



283  
 284



285  
 286  
 287  
 288

Fig.5 a) Local velocity and cellular pattern of detonation propagation in  $D = 25$  mm tube ( $p_0 = 8$

289 kPa); and b) Local velocity of detonation propagation in  $D = 20$  mm tube ( $p_0 = 9$  kPa)

290

291 Local combustion wave velocities were simultaneously acquired together with the smoked  
292 foils. The local velocity results are used to further verify the propagation length  $L_{\text{des}}$  and failure of  
293 the detonation. Figure 5 (a) gives the detonation local velocity and the detonation cellular pattern in  
294 the  $D = 25$  mm circular tube. The length of the smoked foil is 2000 mm, i.e., from  $L = 500\sim 2500$   
295 mm. Figure 5 (a) indicates that, as detonation transmits into the 25-mm circular tube, the detonation  
296 first accelerates to an over-driven detonation ( $L = 500$  mm), and the detonation front consists of  
297 multi-scale cells structure within the next 25 mm distance. As the detonation enters into a small  
298 diameter duct from a larger one, the precursor shock wave reflects from the wall, the shock wave is  
299 then strengthened and develops to a Mach reflection. If the reflection wave is sufficiently strong, a  
300 slightly over-driven detonation may be resulted but quickly relaxed. Similar local velocity evolution  
301 is also seen in Fig. 5 (b) for another tube size  $D = 20$  mm tube at another initial pressure  $p_0 = 9$  kPa.

302 The initially over-driven detonation can always be observed as boundary conditions when a  
303 detonation propagates into an abrupt area change, either as a detonation transmits through an  
304 obstacle, or propagates into a smaller tube from a larger one. For example, Wu and Lee [35]  
305 observed the detonation in  $\text{CH}_4+2\text{O}_2$  is over-driven as it passes through an obstacle. Since we  
306 investigated the detonation propagation behavior in different diameter tubes, and those tubes' inner  
307 diameters are smaller than the test tube, hence the over-driven detonation is inevitable. For  
308 conditions well within the limits, the over-driven detonation quickly develops back to a  
309 self-sustained detonation propagating at about CJ detonation velocity. In the contrary, as the  
310 conditions outside the limits, the initially over-driven detonation relaxes rapidly within few  
311 diameter tubes and the detonation wave continues to decay, and subsequently fail to a fast flame,

312 see Fig. 5. Therefore, the appearance of an initially over-driven detonation does not appear to affect  
313 the propagation behavior in the smaller tubes and that the detonation propagation behavior is mainly  
314 governed by the boundary conditions and the thermodynamics of mixtures in the small tubes.

315 Figure 5 (a) also shows after a short, early transient appearance of an over-driven detonation,  
316 the detonation structure changes quickly to a single-headed spin. As the detonation continues to  
317 decay and the combustion wave's propagation velocity is significantly below the CJ value, the  
318 spinning structure disappears from the foils, which indicates the detonation attenuates into a fast  
319 deflagration wave with low velocity. Therefore, the propagation velocity behavior agrees well with  
320 the cellular pattern evolution. Although a fluctuation of velocity is observed from  $L = 900$  to  $1100$   
321 mm, this velocity fluctuation is totally different from the galloping propagation mode. For a  
322 galloping detonation, the wave first decays to about half CJ detonation velocity from an overdriven  
323 state, and the cellular pattern disappears. Subsequently, this low velocity combustion wave  
324 accelerates once again back to the overdriven state, and the cellular structure recovers. The velocity  
325 of a galloping detonation fluctuates from  $1.5 V_{CJ}$  to  $0.4 V_{CJ}$ . The period of one single cycle of  
326 galloping detonation is about 350 times of tube diameter. In this study, although similar velocity  
327 fluctuation is observed ( $L = 900$  to  $1100$  mm), the cycle is much less than the typical galloping  
328 detonation. Furthermore, it can be seen from the smoked foil that, the single-headed spinning  
329 structure is continuous from  $L = 500$ mm to  $1500$  mm. Therefore, for the distance of  $L = 900$  to  $1100$   
330 mm, it is only some local fluctuation of the propagating detonation, which is also a typical  
331 propagation mode near the limits for an unstable mixture like methane-oxygen. Figure 5 shows that,  
332 the velocity at  $L = 100$  mm is approximately equal to the CJ detonation value of  $\text{CH}_4\text{-2O}_2$  ( $2280$   
333 m/s).

334



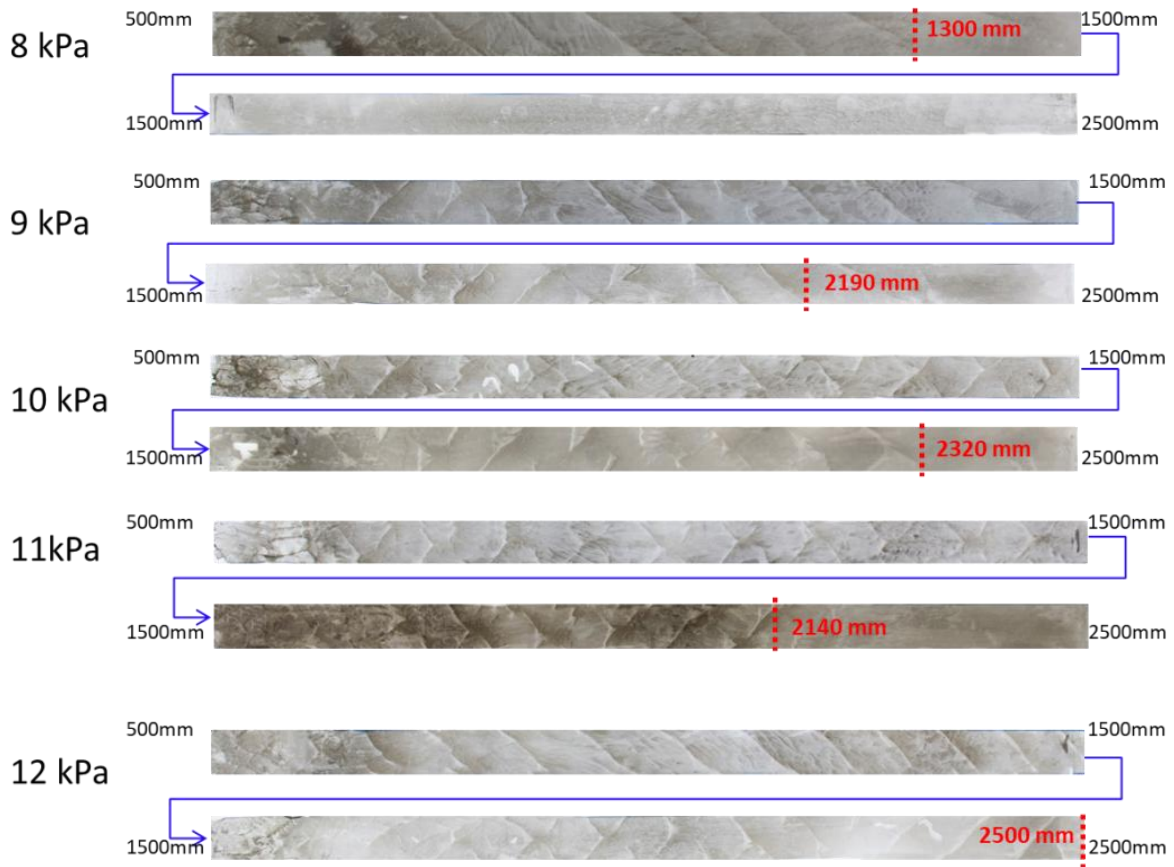


Fig.6 Detonation structure with the variation of  $p_0$  ( $D = 25$  mm)

335

336

337

338

339

340

341

342

343

344

345

346

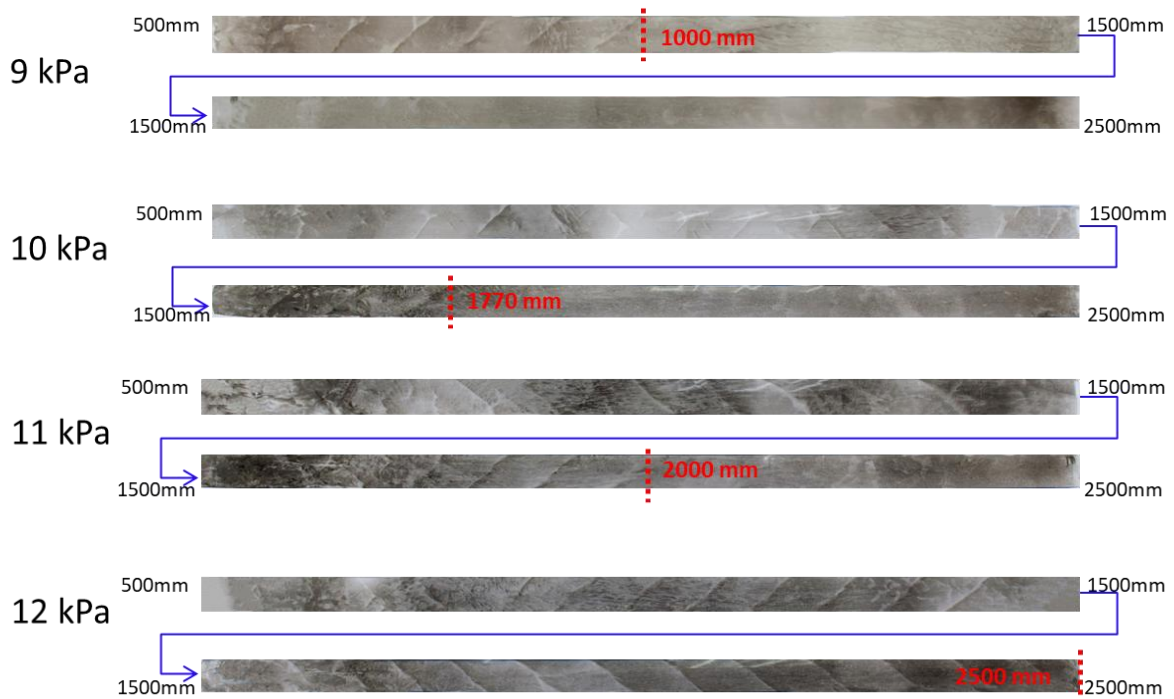
347

348

Figure 6 gives the detonation cellular pattern in the  $D = 25$  mm circular tube for increasing initial pressure from 8 to 12 kPa. At  $p_0 = 9$  kPa, the single-headed spinning structure maintains to  $L = 2190$  mm. In general, with an increase of  $p_0$ ,  $L_{dcs}$  is consequently elongated. Because of the experimental uncertainties, fluctuation of  $L_{dcs}$  can be observed, e.g., as in the  $p_0 = 11$  kPa case. As  $p_0$  increases to 12 kPa, the detonation propagates till the end of the tube ( $L = 2500$  mm) without failure. For  $D = 25$  mm circular tube, the critical pressure is thus  $p_c = 12$  kPa. In some cases, the value of  $L_{dcs}$  at higher initial pressure is smaller than that in lower initial pressure, e.g.,  $L_{dcs}$  in  $p_0 = 11$  kPa is smaller than the result in  $p_0 = 10$  kPa. This variation is a common phenomenon for detonation experiment, especially for unstable mixtures. For these mixtures, detonation initiation is characterized by local explosion; the occurrence of the local explosion has a certain randomness due

349 to its instability. Equivalently, the failure mechanism of a detonation is similar to its initiation; if  
 350 hydrodynamic instabilities are unable to successfully amplify to sustain the propagation of  
 351 detonation, the detonation fails. In the detonation failure process, the interaction between the  
 352 instabilities and the tube wall is complicated, which renders the  $L_{\text{dcs}}$  to vary in a certain degree. The  
 353  $L_{\text{dcs}}$  variation even exists for each shot at the same  $p_0$  as shown previous in Fig. 3. Hence, it is not  
 354 ambiguous that such variation can occur for results when  $p_0$  values are in close proximity, i.e, in  
 355 some cases,  $L_{\text{dcs}}$  is slightly longer at lower  $p_0$ . If the uncertainties discussed in Section 2.2 are taken  
 356 into consideration, these results should be reasonable.

357 Figure 7 shows the detonation propagation behavior in the  $D = 20$  mm tube.  $p_0 = 9$  kPa is the  
 358 initial pressure at which some cellular structure in the 2000-mm long smoked foil can still be  
 359 observed. As  $p_0$  increases to 10 kPa and 11 kPa,  $L_{\text{dcs}}$  increases to 1770 mm and 2000 mm,  
 360 respectively. At  $p_0 = 12$  kPa, a robust single-headed spinning structure throughout the whole  
 361 2000-mm long smoked foil can be found.



363 Fig.7 Detonation structure with the variation of  $p_0$  ( $D = 20$  mm)  
 364

365

366 Figure 8 gives the cellular pattern in the smallest tube considered in this work, i.e.,  $D = 13$  mm.

367 At  $p_0 = 10$  kPa, the detonation fails after  $L = 680$  mm ( $L_{\text{dcs}}/D = 52.3$ ). For the rest of the foil ( $L =$

368  $680$  mm  $\sim 2500$  mm), there is no noticeable structure. At  $p_0 = 11$  kPa,  $L_{\text{dcs}}$  extends to  $1700$  mm

369 ( $L_{\text{dcs}}/D = 130.8$ ). At  $p_0 = 12$  kPa, detonation failure occurs at  $L = 830$  mm. It is interesting to note

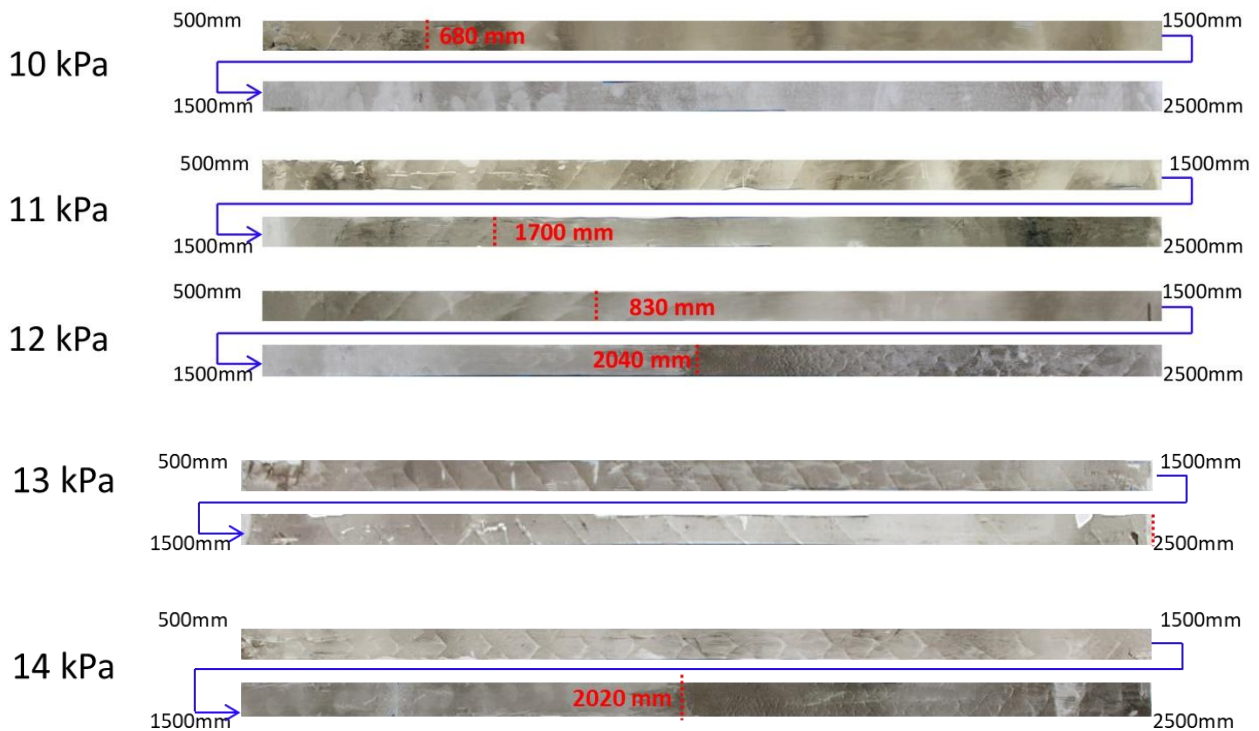
370 that at  $L = 2040$  mm, detonation re-initiation occurs. After the re-initiation, the detonation is

371 over-driven characterized by small fine-scale cells pattern. Subsequently, the detonation decays to

372 the CJ state with normal cellular structure near the end of tube. Later, the cellular pattern turns into

373 spinning again. This observed phenomenon agrees with the galloping detonation that is reported in

374 previous literatures [31, 37, 57, 58].





377

378

Fig.8 Detonation structure with the variation of  $p_0$  ( $D = 13$  mm)

379

380

381

382

383

384

385

386

387

388

389

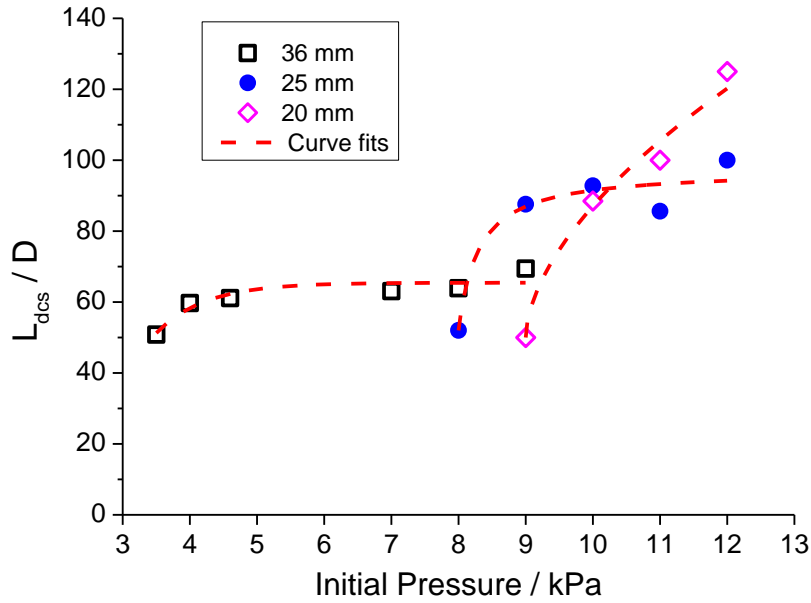
390

It is well known that for a detonation propagating in the galloping mode, the wave first decays to a low-velocity regime from an overdriven state, and later it accelerates back to the overdriven detonation. One cycle period of a single galloping detonation usually needs a length of several hundred of tube inner diameter. At  $p_0 = 12$  kPa, the distance from the failure to re-initiation is 1210 mm,  $L/D = 93$ . As  $p_0$  is slightly increased to 13 kPa, only single-headed spinning structure from  $L = 500$  mm to  $L = 2500$  mm is observed. At  $p_0 = 14$  kPa, galloping detonation with failure and re-initiation behavior can be found, this phenomenon is similar as in the  $p_0 = 12$  kPa case, but with a shorter run-up length. When the initial pressure further increases to 15 kPa, 16 kPa and even 18 kPa, an entire foil with cellular structure can be observed. Hence, for the  $D = 13$ mm tube,  $p_c = 14$  kPa.

391

### 392 3.2 Scaling analysis of detonation failure behavior

393



394 Fig. 9  $L_{dcs}/D$  as a function of  $p_0$  in tubes

394

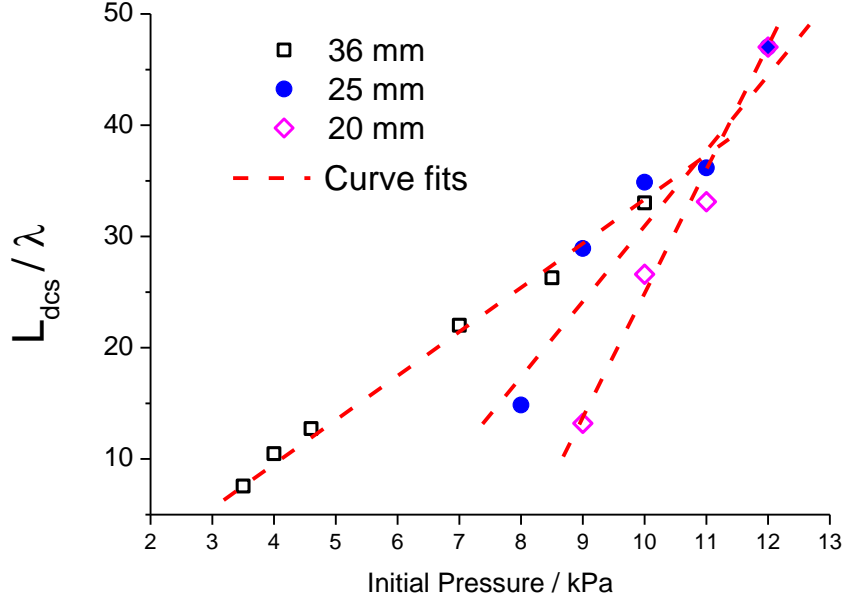
395

396

397 As a detonation propagates in tubes, besides the thermodynamic properties of the mixture, the  
 398 propagation behavior is greatly dependent on the boundary condition. The relationship between the  
 399 detonation propagation behavior and the initial pressure in different diameter tubes is given by Fig.  
 400 9. For the  $D = 13$  mm case, galloping behavior is observed, i.e., after the disappearance of the  
 401 spinning detonation, the deflagration can eventually re-initiate and form an over-driven detonation  
 402 after a certain distance. This criterion that is used to estimate the  $L_{dcs}$  in larger diameter is thus not  
 403 suitable for the  $D = 13$  mm case and hence, only  $D = 36$  mm, 25 mm and 20 mm results are  
 404 considered for discussion in Fig. 9. For the  $D = 36$  mm circular tube, as  $p_0$  increases from 3.5 kPa to  
 405 9 kPa, the value of the ratio between  $L_{dcs}$  and tube inner diameter ( $D$ ) slowly goes up. In other  
 406 words, the detonation propagation is not sensitive to  $p_0$  in the larger inner diameter tube ( $D = 36$   
 407 mm). In the middle-size diameter circular tube, i.e.,  $D = 25$  mm, it is clear that  $L_{dcs}/D$  increases with  
 408 the increase of initial pressure, which indicates a small variation of the initial pressure may cause a

409 long distance for either successful propagation or failure of a detonation. Finally, for the  $D = 20$  mm  
 410 diameter tube, the value of  $L_{\text{dcs}}/D$  increases very abruptly with increasing initial pressure, indicating  
 411  $L_{\text{dcs}}/D$  has a strong dependence on its  $p_0$ .

412



413

414

Fig. 10 Variation of  $L_{\text{dcs}}/\lambda$  with  $p_0$

415

416 As the limits are gradually approaching, the unstable mode of detonation turns into the lowest  
 417 mode of acoustic wave. This acoustic mode is dominated by the tube's characteristic dimension.  
 418 Therefore, the characteristic length scale of the cellular detonation front is correlated with the  
 419 characteristic length scale of the tube at the limit condition. In this work, an attempt is made to  
 420 correlate the two important length scales near the detonation limits used in this work, i.e.,  
 421 detonation cell size  $\lambda$  and  $L_{\text{dcs}}$  as proposed in this work. Figure 10 gives the variation of  $L_{\text{dcs}}/\lambda$  with  
 422 the initial pressure for different tubes. In this work, the detonation cell sizes data are taken from  
 423 Zhang et al. [41]. The relation between cell size and  $p_0$  is given by the power function as follows:

424

$$\lambda = 1127 \cdot p_0 [\text{kPa}]^{-1.229} \quad (1)$$

425

In Fig. 10, it is found that a linear relationship between  $L_{\text{dcs}}/\lambda$  and  $p_0$  for a specific tube can be

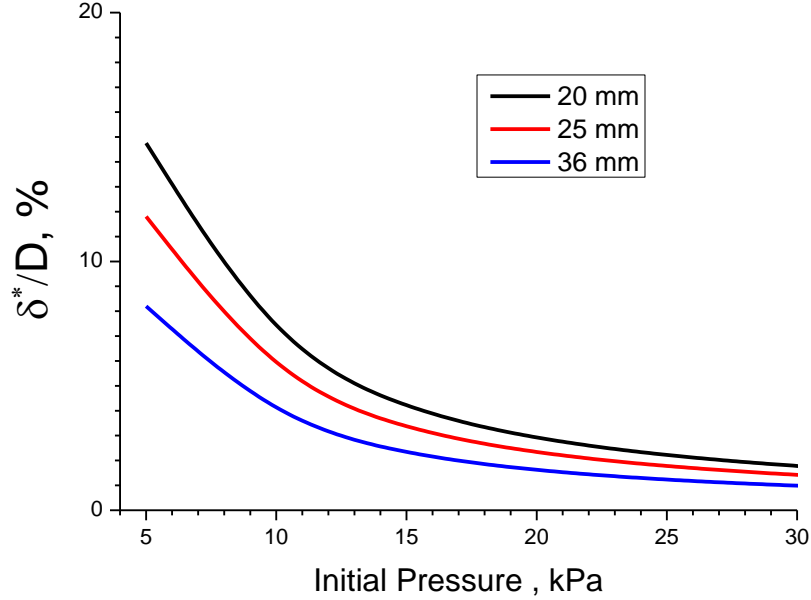
426 obtained. The increase of  $L_{\text{dcs}}/\lambda$  is however more abrupt in the smaller diameter tube, which  
427 confirms again the propagation of detonation is more dependent on the initial pressure in smaller  
428 diameter tube.

429 Another noteworthy observation from Fig. 10 is that for different diameter tubes, the minimum  
430 failing length  $L_{\text{dcs}}$  observed at low initial pressures is of the order of 5 to 14  $\lambda$ . The upper value, i.e.,  
431 is observed for smaller tube diameter  $D$  of which the boundary layer effect not only promotes the  
432 failure, but is found to sustain the wave propagation through flow fluctuations at lead shock  
433 interacting with the boundary. For reference, this minimum  $L_{\text{dcs}}$  range is larger as compared to the  
434 failure length of 3~7  $\lambda$  reported in Radulescu and Lee [53] for the distance traveled by the  
435 attenuated detonation in porous wall tubes before it fails. The difference can be explained as follows.  
436 One should notice that the failure length measured in Radulescu and Lee [53] is defined as the  
437 distance between the locations where the first expansion wave reached the axis to the point where  
438 the detonation fails, while in the present study, it is defined from the beginning of the test tube  
439 section. In addition, the failure mechanism of the present problem and that Radulescu and Lee [53]  
440 are also different. The failure mechanism in Radulescu and Lee is attributed to the losses and mass  
441 divergence into the porous walls, however, in this study, the detonation failure is mainly caused by  
442 tube scale or geometry influencing the effects of boundary layer. Finally, the cell size measurement  
443 and correlation for low pressure conditions generally have a significant uncertainty and this alone  
444 already leads to some discrepancy in the scaling. Although there exist some similarities between the  
445 present work and that of Radulescu and Lee [53] and a similar failure length has been defined, it is  
446 not an attempt here to conclude any quantitative agreement between the two works due to the  
447 aforementioned differences inherent in both phenomena.

448 With decreasing  $p_0$  and  $D$ , the boundary layer displacement thickness increases accordingly

449 [34]. The enlarged boundary layer displacement thickness in the smaller scale tube causes more  
 450 momentum losses through the flow divergence, and faster distribution of curvature over the whole  
 451 detonation front, which eventually results in an earlier failure of the detonation propagation.

452



453

454 Fig. 11 Variation of  $\delta^*$  with  $p_0$  in different tubes

455

456 The boundary layer displacement thickness ( $\delta^*$ ) as a function of  $p_0$  in  $D = 36$  mm, 25 mm and  
 457 20 mm tubes are given in Fig.11.  $\delta^*$  was given by Gooderum [59], which is as follows:

$$458 \quad \delta^* = 0.22x^{0.8} \left( \frac{\mu_e}{\rho_0 V} \right)^{0.2} \quad (2)$$

459 in which,  $x$  represents the reaction zone thickness, Lee [20] and Gao et al. [34] argued  $x = 1.5\lambda$ .  $\mu_e$   
 460 refers to the viscosity,  $V$  is the detonation velocity and  $\rho_0$  is the initial density. Figure 11 shows  
 461 that, with the decrease of initial pressure and the reduction of the tube diameter, the value of  $\delta^*$   
 462 evidently increases.

463 For conditions at which  $\delta^*/D$  is small, either increasing  $D$  or  $p_0$ , the distribution of global  
 464 curvature due to the presence of boundary layer becomes less significant and the failure is thought



465 to be more dominant by the ability to maintain half a detonation cell in the tube. In other words, the  
466 failing length should then be governed primarily by the rate of cell decay or transverse waves  
467 attenuation, i.e., how fast cells evolve or disappear. This is because as detonation suffers more  
468 losses from the wall, the losses to the tube walls are communicated with the entire front more  
469 rapidly, and the failure of detonation occurs more promptly. For  $D = 25$  and  $36$  mm, it is interested  
470 to note in Fig. 9 that the two curves tend to plateau as pressure increases or the boundary layer  
471 thickness relative to the tube diameter decreases.

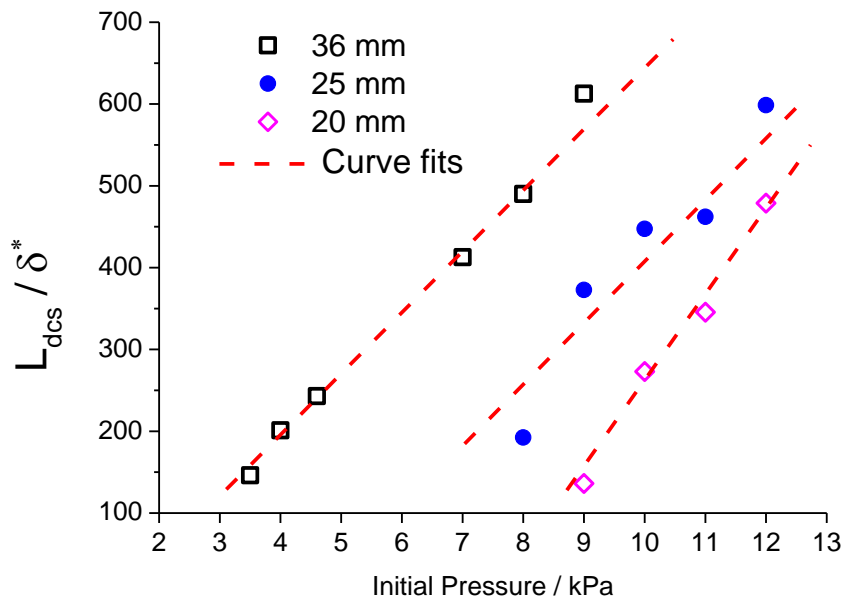
472 It is important to emphasize that the failure length scaling investigated here is valid for  
473 conditions “far” below the limit. In fact, despite some criteria are proposed in the literature, it  
474 remains ambiguous to define exactly the critical detonation limit value due to different unstable  
475 behaviors observed. Due to the inherent unstable behavior of near-limit detonation propagation, it  
476 would be difficult to validate the similar scaling at the proximity to the failure limit. Nevertheless,  
477 we conjecture that there should be a finite failure length at the limit. For the case of unstable  
478 detonations, if the limit phenomenon can be attributed to the ability to maintain half a detonation  
479 cell, the failure length should be corresponding to the inherent condition when a finite cell size  
480 cannot be accommodated. Thus, one cannot determine an increasing failure length toward infinitely  
481 by reducing fractionally a detonation cell as it approaches to the critical limit. Furthermore, the  
482 methane-oxygen mixture considered here is unstable and the cellular front pattern is irregular. The  
483 presence of local instability effects could also affect the scaling at the proximity to the failure limit.  
484 In fact the inherent instabilities are ingredient of different unstable behavior for near-limit  
485 detonation propagation.

486 Figure 11 also shows that at low pressure, the boundary layer thickness growth is comparable  
487 to the tube diameter and engulfs the whole reaction structure. The failure length should be expected

488 to scale with  $D$ . This is indeed observed in Fig. 9. The  $L_{\text{dcs}}/D$  of all tube diameters is approximately  
 489 50 for their lowest initial pressure, at which the boundary layer displacement thickness  $\delta^*$  is  
 490 comparable to the tube diameter  $D$ . At these conditions, the curvature effect due to the lateral mass  
 491 divergence can fail the detonation at a shorter length  $L_{\text{dcs}}$  for smaller tube due to the shorter time it  
 492 takes for the global curvature to distribute over the whole front [53, 60].

493 Similar to Figs. 9 and 10, the relationship between ratio of  $L_{\text{dcs}}/\delta^*$  and the initial pressure is  
 494 given in Fig. 12. The slope of  $L_{\text{dcs}}/\delta^*$  is more steep in the smaller diameter tube, this result  
 495 demonstrates again that the boundary layer displacement thickness in the smaller diameter tube  
 496 greatly affects the earlier extinction of a detonation.

497



498

499 Fig. 12 Variation of  $L_{\text{dcs}}/\delta^*$  with  $p_0$  in different tubes

500

501

502

503

504

505

### 506 3.3 Determination of detonation limits

507

508

Table. 3 Parameters at the critical condition of detonation limits

509

$D/\text{mm}$	$p_c / \text{kPa}$	$\lambda/\text{mm}$	$D/\lambda$
36	9	75.71	0.48
25	12	53.16	0.47
20	12	53.16	0.38
13	15	40.41	0.32

510

511 Table 3 shows the results of the critical pressure ( $p_c$ ), above which a detonation can self-sustain  
512 throughout the entire tube defined by the existence of continuous cellular detonation structure on  
513 the whole foil.  $\lambda$  at the critical pressure is also scaled with its tube inner diameter. For circular tubes,  
514 Lee [20, 61] proposed  $\lambda = \pi \cdot D$  as a limit criterion, where  $\lambda$  represents the transverse wave spacing or  
515 cell size, and  $D$  is the tube diameter, this criterion corresponds to the first onset of single-head spin.  
516 When the structure of detonation is single-headed, the characteristic dimension is the circumference  
517 of the tube, i.e.,  $\pi \cdot D$ . This criterion was verified by other researchers, e.g., Dupré et al. [62], Yoshida  
518 et al. [36], Fischer et al. [63] and Gao et al. [30]. As can be seen from Table 3,  $D/\lambda \sim 0.41$ , which  
519 approaches well to the detonation limit criterion  $\lambda = \pi \cdot D$  within the experimental uncertainties.  
520 Generally  $\lambda$  is inversely proportional to the initial pressure, i.e.,  $\lambda \sim p_0^{-1}$ . Given the scaling  $\lambda = a \cdot D$   
521 where the parameter  $a > 1$ , it indirectly demonstrates that the limit is more sensitive to  $p_0$  governing  
522 the detonation structure than the effect of tube scale.

523 In summary, some remarks can be made with regards to the effects of  $p_0$  on the detonation  
524 limit phenomenon. It is perhaps well established that  $p_0$  affects the dynamic detonation parameters.  
525 In this study, the test mixture is  $\text{CH}_4\text{-2O}_2$ , which is considered an unstable mixture (i.e., with  
526 irregular cellular pattern). For unstable mixtures, the detonation propagation limit criterion  $\lambda = \pi \cdot D$   
527 holds in macro-scale ducts. Yoshida et al. [36] proposed a factor ( $\alpha$ ) that determines the detonation

528 limit, i.e.,  $\alpha = \pi \cdot D / \lambda$ . When  $\alpha$  equals to 1, the detonation limit is approached. If  $\alpha < 1$ , the  
529 single-headed spinning structure is observed and afterwards this structure disappears eventually,  
530 which indicates detonation failure. It is well observed that with the decreasing of  $p_0$ , the detonation  
531 cell size  $\lambda$  increases exponentially, which renders the value of  $\alpha$  much smaller than 1, and the  
532 detonation failure occurs. The ability of detonation propagation in tubes thus depends on the ability  
533 of the mixture to generate cells or transverse waves within, of which the initial pressure is one of  
534 the governing parameter.

535 From a purely thermodynamic and chemical kinetic point-of-view, although it could be a  
536 secondary effect, decreasing initial pressure reduces the detonation strength and elongates the  
537 induction zone of the detonation structure. The latter also explains why the cell size decreases as  
538 initial pressure increases. For a fixed diameter tube, it leads the detonation structure more  
539 susceptible to losses making it more prompt to failure when the boundary layer thickness becomes  
540 comparable to the reaction zone thickness. The initial pressure also affects the boundary layer  
541 displacement thickness  $\delta^*$ . The  $\delta^*/D$  appears to be a significant parameter to explain different trends  
542 shown in Fig. 9 and Fig. 10. The initial pressure, which governs the value of  $\delta^*/D$ , could therefore  
543 dictate whether the failure mechanism is primarily dominated by the lateral mass divergence  
544 resulting a global frontal curvature or the rate of cells attenuation.

545

#### 546 **4. Conclusions**

547 In this study, the dynamic behavior of detonation propagation and failure at the limits was  
548 investigated experimentally. Simultaneous velocity measurement and smoked foils were used to  
549 observe velocity deficits and the evolution of the detonation cellular structure, from which limits  
550 (i.e., critical pressures) were defined. An alternate characteristic length ( $L_{dcs}$ ), defined as the length

551 from the start of the test tube section to the location where no cellular detonation structure, is  
552 recorded with varying initial pressure in four different inner diameter tubes, i.e.,  $D = 36, 25, 20$  and  
553  $13$  mm. The quantitative relation between the cellular detonation propagation distance, the  
554 thermodynamic properties of the mixture, and the tube geometry were explored. The results show  
555 that  $L_{\text{dcs}}$  generally decreases with decreasing initial mixture pressure, and it decreases faster in  
556 smaller diameter tubes. In this study, the detonation galloping mode is only observed in the  $D = 13$   
557 mm diameter tube. With the increase of  $p_0$ , the length of the galloping cycle is reduced. By scaling  
558  $L_{\text{dcs}}$  with tube inner diameter ( $D$ ) and detonation cell size ( $\lambda$ ), it is found that the decrease of  $L_{\text{dcs}}/D$   
559 and  $L_{\text{dcs}}/\lambda$  are more abrupt in smaller diameter tubes with decreasing initial pressure. It thus suggests  
560 that the detonation propagation dynamics is more sensitive to the initial pressure in the smaller  
561 diameter tube. The latter is explained according to the argument of the significant boundary layer  
562 displacement thickness growth at low initial pressure and the curvature due to the lateral mass  
563 divergence. The distribution rate of global curvature over the whole detonation front due to the  
564 boundary layer effect is faster in smaller tube and thus it leads to a more abrupt decrease sensitive to  
565 initial pressure.

566 For increasing pressure closer to the failure limit from below, the boundary layer displacement  
567 thickness is becoming less comparable to the tube diameter. The failing length no longer scales with  
568  $D$  based on the global curvature. The failure mechanism can be thought to be more dominant by the  
569 rate of transverse wave attenuation or cell disappearance. Lastly, by analyzing the critical condition  
570 of detonation limits in different tubes, once again it confirms that  $\lambda = \pi \cdot D$  provides an appropriate  
571 limit criterion for detonation propagation in accordance with the literature.

572

573 **Acknowledgments**

574 This work is supported by the National Natural Science Foundation of China – China (Grant Nos.:  
575 11772199 and 91741114).

576  
577

---

<b>Nomenclature</b>	
CJ	Chapman-Jouguet
$V_{CJ}$	CJ detonation velocity
$D$	Tube inner diameter
$p_c$	Critical pressure for detonation limits
$p_0$	Initial pressure
$T_0$	Initial temperature
$\lambda$	Detonation cell size
$\delta^*$	Boundary layer displacement thickness
$L$	Length of tube
$L_{dcs}$	Maximum length of detonation cellular structure
AC	Annular channel
CT	Circular tube
$H$	Height of channel
$\chi$	Stability parameter
$\varphi$	Equivalence ratio

---

578  
579  
580

581 **References:**

- 582 [1] Shepherd J E. Detonation in gases. Proc Combust Inst 2009;32:83-98.
- 583 [2] Ciccarelli G , Dorofeev S. Flame acceleration and transition to detonation in ducts. Prog Energ  
584 Combust 2008;34:499-550.
- 585 [3] Wolanski P. Detonative propulsion. Proc Combust Inst 2013;34:125-58.
- 586 [4] Zhang B , Bai C H. Critical energy of direct detonation initiation in gaseous fuel-oxygen  
587 mixtures. Safety Sci 2013;53:153-9.
- 588 [5] Roy G D, Frolov S M, Borisov A A , Netzer D W. Pulse detonation propulsion: challenges,  
589 current status, and future perspective. Prog Energ Combust 2004;30:545-672.

- 590 [6] Mehrjoo N, Portaro R , Ng H D. A technique for promoting detonation transmission from a  
591 confined tube into larger area for pulse detonation engine applications. *Propulsion and Power*  
592 *Research* 2014;3:9-14.
- 593 [7] Changxin P, Wei F, Qun Z, Cheng Y, Wenjuan C , Chuanjun Y. Experimental study of an  
594 air-breathing pulse detonation engine ejector. *Exp Therm Fluid Sci* 2011;35:971-7.
- 595 [8] Rocourt X, Sochet I, Gillard P, Faubert F , Dagaut P. Detonability of simple and representative  
596 components of pyrolysis products of kerosene: pulsed detonation engine application. *Shock*  
597 *Waves* 2005;14:283-91.
- 598 [9] Uemura Y, Hayashi A K, Asahara M, Tsuboi N , Yamada E. Transverse wave generation  
599 mechanism in rotating detonation. *Proc Combust Inst* 2013;34:1981-9.
- 600 [10] Schwer D , Kailasanath K. Fluid dynamics of rotating detonation engines with hydrogen and  
601 hydrocarbon fuels. *Proc Combust Inst* 2013;34:1991-8.
- 602 [11] Zhou R , Wang J P. Numerical investigation of flow particle paths and thermodynamic  
603 performance of continuously rotating detonation engines. *Combust Flame* 2012;159:3632-45.
- 604 [12] Fang Y, Zhang Y, Deng X , Teng H. Structure of wedge-induced oblique detonation in  
605 acetylene-oxygen-argon mixtures. *Phys Fluids* 2019;31.
- 606 [13] Zhang Y, Fang Y, Ng H D , Teng H H. Numerical investigation on the initiation of oblique  
607 detonation waves in stoichiometric acetylene-oxygen mixtures with high argon dilution.  
608 *Combust Flame* 2019;204:391-6.
- 609 [14] Yang P F, Teng H H, Ng H D , Jiang Z L. A numerical study on the instability of oblique  
610 detonation waves with a two-step induction-reaction kinetic model. *Proc Combust Inst*  
611 2019;37:3537-44.
- 612 [15] Teng H H , Jiang Z L. On the transition pattern of the oblique detonation structure. *J Fluid*

- 613 Mech 2012;713:659-69.
- 614 [16] Teng H H, Jiang Z L , Ng H D. Numerical study on unstable surfaces of oblique detonations. J  
615 Fluid Mech 2014;744:111-28.
- 616 [17] Teng H H, Ng H D, Li K, Luo C T , Jiang Z L. Evolution of cellular structures on oblique  
617 detonation surfaces. Combust Flame 2015;162:470-7.
- 618 [18] Teng H, Ng H D , Jiang Z. Initiation characteristics of wedge-induced oblique detonation  
619 waves in a stoichiometric hydrogen-air mixture. Proc Combust Inst 2017;36:2735-42.
- 620 [19] Yang P, Teng H, Jiang Z , Ng H D. Effects of inflow Mach number on oblique detonation  
621 initiation with a two-step induction-reaction kinetic model. Combust Flame 2018;193:246-56.
- 622 [20] Lee J H S, The detonation phenomenon, Cambridge University Press, 2008.
- 623 [21] Ishii K , Gronig H. Behavior of detonation waves at low pressures. Shock Waves  
624 1998;8:55-61.
- 625 [22] Haloua F, Brouillette M, Lienhart V , Dupre G. Characteristics of unstable detonations near  
626 extinction limits. Combust Flame 2000;122:422-38.
- 627 [23] Ishii K, Itoh K , Tsuboi T. A study on velocity deficits of detonation waves in narrow gaps.  
628 Proc Combust Inst 2002;29:2789-94.
- 629 [24] Chao J, Ng H D , Lee J H S. Detonability limits in thin annular channels. Proc Combust Inst  
630 2009;32:2349-54.
- 631 [25] Kitano S, Fukao M, Susa A, Tsuboi N, Hayashi A K , Koshi M. Spinning detonation and  
632 velocity deficit in small diameter tubes. Proc Combust Inst 2009;32:2355-62.
- 633 [26] Camargo A, Ng H D, Chao J , Lee J H S. Propagation of near-limit gaseous detonations in  
634 small diameter tubes. Shock Waves 2010;20:499-508.
- 635 [27] Ishii K , Monwar M. Detonation propagation with velocity deficits in narrow channels. Proc



- 636 Combust Inst 2011;33:2359-66.
- 637 [28] Sadahira K, Kitawaki Y, Inaba T, Susa A, Matsuoka K, Johzaki T , Endo T, Velocity Deficits  
638 of Ar and He diluted H<sub>2</sub>-O<sub>2</sub> System in Small Diameter Tubes, Taipei, Taiwan, 2013.
- 639 [29] Lee J H S, Jesuthasan A , Ng H D. Near limit behavior of the detonation velocity. Proc  
640 Combust Inst 2013;34:1957-63.
- 641 [30] Gao Y, Ng H D , Lee J H S. Minimum tube diameters for steady propagation of gaseous  
642 detonations. Shock Waves 2014;24:447-54.
- 643 [31] Gao Y, Ng H D , Lee J H S. Experimental characterization of galloping detonations in unstable  
644 mixtures. Combust Flame 2015;162:2405-13.
- 645 [32] Gao Y, Ng H , Lee J H S. Near-limit propagation of gaseous detonations in thin annular  
646 channels. Shock Waves 2017;27:199-207.
- 647 [33] Gao Y, Lee J H S , Ng H D. Velocity fluctuation near the detonation limits. Combust Flame  
648 2014;161:2982-90.
- 649 [34] Gao Y, Zhang B, Ng H D , Lee J H S. An experimental investigation of detonation limits in  
650 hydrogen-oxygen-argon mixtures. Int J Hydrogen Energ 2016;41:6076-83.
- 651 [35] Wu Y W , Lee J H S. Stability of spinning detonation waves. Combust Flame  
652 2015;162:2660-9.
- 653 [36] Yoshida K, Hayashi K, Morii Y, Murakami K, Tsuboi N , Hayashi A K. Study on Behavior of  
654 Methane/Oxygen Gas Detonation Near Propagation Limit in Small Diameter Tube: Effect of  
655 Tube Diameter. Combust Sci Technol 2016;188:2012-25.
- 656 [37] Jackson S I , Short M. Scaling of Detonation Velocity in Cylinder and Slab Geometries for  
657 Ideal, Insensitive and Non-Ideal Explosives. J Fluid Mech 2015;773:224-66.
- 658 [38] Wang L, Ma H, Shen Z, Xue B, Cheng Y , Fan Z. Experimental investigation of

659 methane-oxygen detonation propagation in tubes. *Appl Therm Eng* 2017;123:1300-7.

660 [39] Zhang B, Liu H , Yan B J. Effect of acoustically absorbing wall tubes on the near-limit  
661 detonation propagation behaviors in a methane-oxygen mixture. *Fuel* 2019;236:975-83.

662 [40] Zhang B, Liu H , Wang C. Detonation propagation limits in highly argon diluted  
663 acetylene-oxygen mixtures in channels. *Exp Therm Fluid Sci* 2018;90:125-31.

664 [41] Zhang B, Liu H, Wang C , Yan B J. An experimental study on the detonability of gaseous  
665 hydrocarbon fuel - oxygen mixtures in narrow channels. *Aerosp Sci Technol* 2017;69:193-200.

666 [42] Zhang B, Liu H , Wang C. Detonation velocity behavior and scaling analysis for  
667 ethylene-nitrous oxide mixture. *Appl Therm Eng* 2017;127:671-8.

668 [43] Zhang B. The influence of wall roughness on detonation limits in hydrogen-oxygen mixture.  
669 *Combust Flame* 2016;169:333-9.

670 [44] Zhang B, Pang L , Gao Y. Detonation limits in binary fuel blends of methane/hydrogen  
671 mixtures. *Fuel* 2016;168:27-33.

672 [45] Zhang B, Pang L, Shen X B , Gao Y. Measurement and prediction of detonation cell size in  
673 binary fuel blends of methane/hydrogen mixtures. *Fuel* 2016;172:196-9.

674 [46] Zhang B, Shen X B, Pang L , Gao Y. Methane-oxygen detonation characteristics near their  
675 propagation limits in ducts. *Fuel* 2016;177:1-7.

676 [47] Zhang B, Shen X B, Pang L , Gao Y. Detonation velocity deficits of H<sub>2</sub>/O<sub>2</sub>/Ar mixture in  
677 round tube and annular channels. *Int J Hydrogen Energ* 2015;40:15078-87.

678 [48] Zhang B, Liu H , Yan B J. Investigation on the detonation propagation limit criterion for  
679 methane-oxygen mixtures in tubes with different scales. *Fuel* 2019;239:617-22.

680 [49] Zhang B, Liu H , Yan B J. Velocity behavior downstream of perforated plates with large  
681 blockage ratio for unstable and stable detonations. *Aerosp Sci Technol* 2019;86:236-43.

- 682 [50] Zhang B, Liu H , Li Y C. The effect of instability of detonation on the propagation modes near  
683 the limits in typical combustible mixtures. *Fuel* 2019;253:305-10.
- 684 [51] Zhang B , Liu H. The effects of large scale perturbation-generating obstacles on the  
685 propagation of detonation filled with methane-oxygen mixture. *Combust Flame*  
686 2017;182:279-87.
- 687 [52] Fay J A. Two-dimensional gaseous detonations: velocity deficit. *Phys Fluids* 1959;2:283.
- 688 [53] Radulescu M I , Lee J H S. The failure mechanism of gaseous detonations: Experiments in  
689 porous wall tubes. *Combust Flame* 2002;131:29-46.
- 690 [54] Xiao Q, Chang J, La Fleche M, Wang Y , Radulescu M I, Propagation Characteristics of  
691  $2\text{H}_2/\text{O}_2/2\text{Ar}$  Detonations in Channels with Constant Area Divergence, 26th International  
692 Colloquium on the Dynamics of Explosions and Reactive Systems, Boston, USA, 2017.
- 693 [55] Radulescu M I, The propagation and failure mechanism of gaseous detonation: experiments in  
694 porous-walled tubes, McGill University. 2003.
- 695 [56] Ng H D, The effect of chemical reaction kinetics on the structure of gaseous detonations,  
696 McGill University. 2005.
- 697 [57] Tsuboi N, Morii Y , Hayashi A K. Two-dimensional numerical simulation on galloping  
698 detonation in a narrow channel. *Proc Combust Inst* 2013;34:1999-2007.
- 699 [58] Elsworth J E, Shuff P J , Ungut A. "Gallopig" gas detonations in the spherical mode. In *Prog.*  
700 *Astronaut. Aeronaut* 1984;94:130-50.
- 701 [59] Gooderum P B. 1958. An experimental study of the turbulent boundary layer on a shock-tube  
702 wall. National Advisory Committee for Aeronautics Tech Note 4243, Langley Aeronautical  
703 Laboratory
- 704 [60] Bdzil J B , Stewart D S. Time-dependent two-dimensional detonation: the interaction of edge

- 705 rarefactions with finite-length reaction zones. *J Fluid Mech* 1986;171:1-26.
- 706 [61] Lee J H S. Dynamic parameters of gaseous detonations. *Annu Rev Fluid Mech*  
707 1984;16:311-36.
- 708 [62] Dupré G, Knystautas R , Lee J H. Near-limit propagation of detonation in tubes. *Progress in*  
709 *Astronautics and Aeronautics* 1986;106:244-59.
- 710 [63] Fischer J, Liebner C, Hieronymus H , Klemm E. Maximum safe diameters of microcapillaries  
711 for a stoichiometric ethene/oxygen mixture. *Chem Eng Sci* 2009;64:2951-6.  
712